THE JOURNAL OF PHYSICAL CHEMISTRY A

Article

pubs.acs.org/JPCA

Nonadiabatic Eigenfunctions Can Have Amplitude, Signed Conical Nodes, or Signed Higher Order Nodes at a Conical Intersection with Circular Symmetry

Published as part of The Journal of Physical Chemistry virtual special issue "Veronica Vaida Festschrift".

Peter W. Foster and David M. Jonas*

Department of Chemistry and Biochemistry, University of Colorado, Boulder, Colorado 80309-0215, United States

Supporting Information

ABSTRACT: Numerically exact nonadiabatic eigenfunctions are computed for a two-dimensional conical intersection with circular symmetry, for which a pseudorotation quantum number is conserved and all eigenstates are doubly degenerate. In the calculations reported here, the conical intersection is submerged, with energy below the zero point level. The complete real-valued vibrational-electronic eigenfunctions are visualized using Hunter's exact factorization for the total vibrational amplitude factor and color for the electronic factor. The zero-point levels have nonzero amplitude at the conical intersection. Nodes in the degenerate nonadiabatic eigenfunctions are classified as accidental if they can be moved or removed by a change in degenerate basis and as essential if they cannot. An integer electronic index defines the order of the nodes for nonadiabatic eigenfunctions by simple closed counterclockwise line integrals. Higher eigenstates can have accidental conical nodes around the conical intersection and essential nodes of varying circular orders at the conical intersection. The signs of the essential nodes are all opposite the sign of the conical intersection and the signed node orders obey sum rules. Even for submerged conical intersections, the appearance of the exact eigenstates motivates use of signed, half-odd-integral, pseudorotation quantum numbers j. Essential nodes of absolute order $(|j| - 1/2)$ are located on the conical intersection for $|j|$ greater than or equal to 3/2. The eigenfunctions around essential first order nodes are right circular cones with their vertex at the conical intersection.

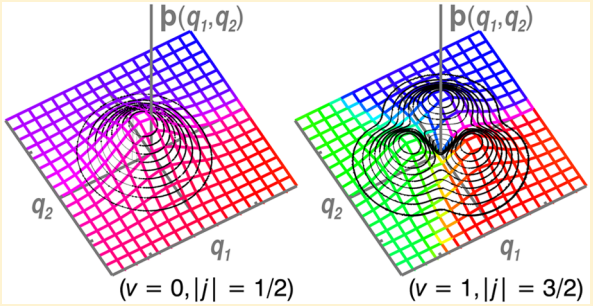

INTRODUCTION

Soon after Born and Oppenheimer published their fundamental paper on the separation of electronic and vibrational motions,[1] von Neumann and Wigner established that potential energy surfaces in polyatomic molecules are likely to intersect, which can cause a breakdown of the Born−Oppenheimer approximation.[2] The intersections between surfaces have the geometry of a right elliptical cone. Later, Jahn and Teller proved that degenerate electronic states in many point groups would split their degeneracy by lowering their symmetry away from a conical intersection at the high symmetry geometry.[3] Moffit and Liehr treated a conical intersection with circular symmetry in the nonadiabatic limit where the vibrational-electronic coupling and vibrational forces are comparable.[4] Later, Longuet-Higgins et al. analyzed the adiabatic limit for the same model,[5] finding two vibrational periods per electronic period (a precursor of Berry's geometric phase[6,7]) and a half-odd-integer quantum number[8] for what is now called pseudorotation.[9] Conical intersections and their higher dimensional analogues are now appreciated as widely important for photochemistry.[10−14] Because of their symmetry, Jahn−Teller conical intersections are the simplest type.[15−18]

In the static Jahn−Teller effect, the molecule effectively adopts one of a few equivalent low symmetry equilibrium geometries.[15,18] For a dynamical Jahn−Teller effect, interconversion between equivalent low symmetry geometries is feasible and the average structure can recover the higher symmetry[15,18,19] even if the high symmetry geometry has zero probability. When the Jahn−Teller coupling is also weak,[15] the adiabatic potential energy of the Jahn−Teller conical intersection becomes energetically accessible. However, the lowest energy eigenstates of such systems are in a deeply quantum regime of nonadiabatic dynamics, where the concept of a potential surface should be abandoned[8] and semiclassical and adiabatic intuition fail. Weak dynamical Jahn−Teller effects are so common in molecules that it took over a decade to find experimental evidence for the Jahn−Teller effect.[19] This paper discusses wave functions at the high symmetry geometry under weak dynamical Jahn−Teller coupling for the highest symmetry conical intersection.

Received: July 19, 2017
Revised: September 11, 2017
Published: September 26, 2017

DOI: 10.1021/acs.jpca.7b07140
J. Phys. Chem. A 2017, 121, 7401−7413

For nonadiabatic systems, Hunter developed a factorization that parallels the Born−Oppenheimer factorization in many ways. In Hunter's exact factorization,[20,21] each normalized eigenfunction $\psi_m(\mathbf{r},\mathbf{q})$ is written as a product of a marginal vibrational factor,

$$Þ_m(\mathbf{q}) = \sqrt{\int \psi_m^*(\mathbf{r},\mathbf{q})\psi_m(\mathbf{r},\mathbf{q})d\mathbf{r}} \quad (1)$$

and a conditional electronic factor

$$K_m(\mathbf{r};\mathbf{q}) = \psi_m(\mathbf{r},\mathbf{q}) / Þ_m(\mathbf{q}) \quad (2)$$

Each vibrational factor is square-normalized with respect to integration over all vibrational coordinates. Each conditional electronic factor is square-normalized, as a function of the electronic coordinates $\mathbf{r}$, for every set of vibrational coordinates $\mathbf{q}$ on which it depends parametrically. This factorization has been useful for nonadiabatic problems[22,23] and extended to treat nonadiabatic dynamics.[24,25] Reference 26 exploited the fact that, if only two electronic states (x and y) are involved, the electronic factor at each point in the vibrational coordinate space can be fully specified (in character and phase) by the electronic angle

$$\begin{aligned}\Theta_m(\mathbf{q}) &\equiv \text{atan2}(\langle y|\psi_m\rangle, \langle x|\psi_m\rangle) \\ &= \text{atan2}(\langle y|K_m\rangle, \langle x|K_m\rangle)\end{aligned} \quad (3)$$

where atan2 returns angles over a 2π range. $\Theta_m(\mathbf{q})$ does not depend on the division in eq 2. Representing the positive vibrational factor by amplitude contours and the signed electronic factor by color (a colored exact factorization) allows complete visualization of real-valued nonadiabatic eigenfunctions with a single map.[26]

Although the structure of marginal vibrational and conditional electronic factors parallels the Born−Oppenheimer factorization, Hunter's exact factorization differs from the Born−Oppenheimer factorization in two key ways: first, nonadiabatic electronic factors can be different for each vibrational-electronic eigenstate; second, nonadiabatic vibrational factors need not have nodes. The Born−Oppenheimer approximation requires a sum of vibrational-electronic products for such nonadiabatic states. In both factorizations, the separate factors may not be allowed wave functions; the exact factors may not have continuous derivatives in the adiabatic limit and the Born−Oppenheimer factors may not be single-valued around a conical intersection (Berry phase). The Born−Oppenheimer factorization is quite naturally connected to spectroscopy measurements that depend on one-electron operators (which can image one electronic factor in a sum), while Hunter's exact factorization is natural for diffraction and imaging measurements that probe the total vibrational probability density.[26]

For diatomics, the division used to define the electronic factor is made possible by the absence of nodes in the vibrational factor $Þ_m$.[27] This occurs because $Þ_m$ is the square root of the total vibrational probability density obtained by tracing over the electronic states and because the vibrational amplitudes on different electronic states are unlikely to all have a zero at exactly the same place unless required by symmetry.[28] As a result, nodes in the dominant adiabatic wave function are avoided by a continuous change in electronic character in which a nonadiabatically coupled state "peeks through" at and around the dominant node. This nodeless property is exploited in use of the exact factorization for nonadiabatic dynamics.[24,25] Recently, it has been shown that accidental nodes can occur if the dimensionality of the vibrational coordinate space equals or exceeds the number of coupled electronic states.[26] Such nodes have the shape of a right elliptical cone with the node at the vertex (conical nodes). In principle, this result does not contradict the absence of true vibrational nodes for an infinite number of coupled electronic states. In practice, it suggests observable weakly avoided vibrational zeroes of low dimensionality in the total vibrational probability density.[26]

This paper uses the colored exact factorization to examine the nodes of exact nonadiabatic eigenfunctions at a conical intersection with circular symmetry. The conical intersections studied here are submerged below the zero point energy. This high symmetry model is identical to that studied by Moffit and Liehr,[4] by Longuet-Higgins et al.,[5] and by Judd.[29] It is also a higher symmetry version of the submerged conical intersection used to model experiments that measured loss of electronic alignment on a ∼100 fs time scale[30,31] and slower loss of electronic coherence[32] in a doubly degenerate electronic state of a silicon naphthalocyanine.

Recent work has discussed the adiabatic effects required to generate nonadiabatic wave function amplitude at a conical intersection in terms of compensating divergent nonadiabatic corrections[33] or compensating discontinuities in the adiabatic factors.[23] The amplitude and phase behavior around a conical intersection are critical for nonadiabatic tunneling.[34−36] The nonadiabatic eigenfunctions obtained here are consistent with conjectures about nonzero amplitude at a conical intersection.[23,33] At the conical intersection studied here, essential nodes in the nonadiabatic eigenfunctions can be required by symmetry. It will be shown that these conical nodes and higher order nodes have lowest radial exponents determined by the pseudorotation quantum number.

THEORY

Using the diabatic electronic basis $\{|x\rangle,|y\rangle\}$ and dimensionless normal coordinates, the circularly symmetric Jahn−Teller Hamiltonian[37] is (divided by $\hbar$)

$$\begin{aligned}\hat{\mathbf{H}} = &[(1/2)\omega(\hat{p}_1^2 + \hat{q}_1^2) + (1/2)\omega(\hat{p}_2^2 + \hat{q}_2^2)]\hat{\mathbf{I}} \\ &+ \omega d\hat{q}_1[|x\rangle\langle x| - |y\rangle\langle y|] + \omega d\hat{q}_2[|x\rangle\langle y| + |y\rangle\langle x|]\end{aligned} \quad (4)$$

where ω is the vibrational frequency, $\hat{q}_i$ and $\hat{p}_i$ are the dimensionless normal coordinate position and momentum operators (i = 1 or 2) for asymmetric vibrations, $\hat{\mathbf{I}} = |x\rangle\langle x| + |y\rangle\langle y|$ is the electronic identity operator, and d is the vibrational displacement. The first line is an isotropic two-dimensional harmonic oscillator Hamiltonian. The second line contains vibrational-electronic couplings. This Hamiltonian separately commutes with two mutually noncommuting reflection operators σ_v and σ_d, and thus all energy eigenvalues are doubly degenerate.[38] These reflection operators have the following effects[32] on the asymmetric coordinates and the electronic basis states:

$$\sigma_v q_1 = +q_1, \quad \sigma_v q_2 = -q_2 \quad (5a)$$

$$\sigma_v|x\rangle = +|x\rangle, \quad \sigma_v|y\rangle = -|y\rangle \quad (5b)$$

and

$$\sigma_d q_1 = -q_1, \quad \sigma_d q_2 = +q_2 \quad (5c)$$

$$\sigma_d|x\rangle = +|y\rangle, \quad \sigma_d|y\rangle = +|x\rangle \quad (5d)$$

DOI: 10.1021/acs.jpca.7b07140
J. Phys. Chem. A 2017, 121, 7401−7413

Eigenstates can be chosen so that they are simultaneously eigenstates of the Hamiltonian and of either reflection operator.

Figure 1 shows the two adiabatic potential energy surfaces obtained by neglecting the momentum operators and diagonalizing the resulting electronic Hamiltonian at each coordinate. Color indicates the coordinate-dependent electronic character and phase for each surface, which have been chosen for maximum continuity. The two adiabatic potential surfaces have circular symmetry, a Jahn–Teller conical intersection at the origin, and a lower surface minimum below it at $V_{min} = -(1/2)\omega d^2 = -(D\omega)$. $(D\omega)$ is known as the Jahn–Teller stabilization energy,[39−41] and its definition exactly parallels that of the Marcus reorganization energy[42] for a totally symmetric coordinate. In Figure 1, the zero point energy is marked by black rings on the potential energy surfaces. In some sense, only about half of the zero point energy is available to each of the two coordinates. Even so, the conical intersection is submerged below the zero point energy. The light blue to orange color discontinuities indicate π phase shifts along $q_2 = 0$ after one circuit around the conical intersection. The location of this discontinuity is arbitrary, but the necessity for such a "cut" was first noted by Mead and Truhlar,[43] and it can be regarded as a consequence of Berry's geometric phase.[6]

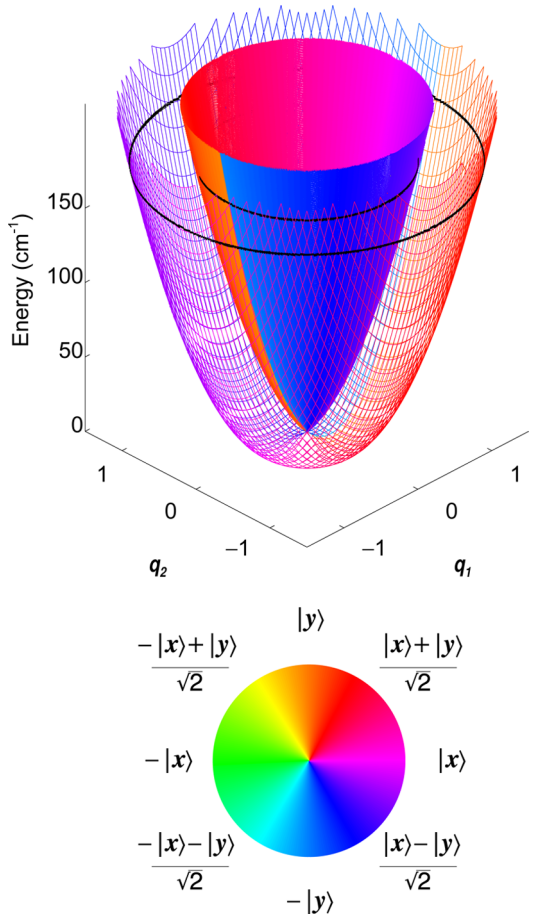

Figure 1. Adiabatic potential energy surfaces and coordinate dependent electronic character for the model Hamiltonian. The vibrational frequency is ω = 200 cm^{-1} and the Jahn–Teller stabilization energy is $(D\omega)$ = 10 cm^{-1}. Color represents adiabatic electronic character $|\psi_{elec}(q_1,q_2)\rangle$ according to the color wheel at the bottom. The conical intersection at $q_1 = q_2 = 0$ and $E = 0$ is submerged below the zero-point energy of E_{zp} = 181 cm^{-1} (black curve). The lower adiabatic potential surface descends from the conical intersection to its minimum at $E_{min} = -(D\omega)$ around the circle $(q_1^2 + q_2^2)^{1/2} = d$. An adiabatic phase discontinuity in electronic character must occur for both the inner (solid) and outer (mesh) surfaces, is arbitrarily placed along $q_2 = 0$ and is visible as an angular color discontinuity from orange $|y\rangle$ to light blue $-|y\rangle$. Starting and stopping at the discontinuity, a counterclockwise path around either adiabatic surface rotates halfway around the color wheel in a counterclockwise direction.

Longuet-Higgins et al. discovered that the circularly symmetric Jahn–Teller Hamiltonian can be extended to reveal a rigorously conserved quantum number[5] for what is now called pseudorotation.[9] Subsequent work by Hougen[37] and Oka[44] has emphasized that the form of this quantum number depends on the phase convention (it is not the total angular momentum as stated in refs 4 and 5, see ref 8). In order to use the current standard phase conventions, we extend the Hamiltonian by regarding the electronic states $|x\rangle$ and $|y\rangle$ as $-\cos\theta$ and $-\sin\theta$ [these choices most resemble the standard doubly degenerate 2D particle in a square box states (n_x,n_y) = (2,1) and (1,2), respectively]. These two electronic states span $\lambda = \pm 1$ within a complete set of electronic states of the form $\exp(i\lambda\theta)$, where θ is a continuous electronic rotation angle and λ is the electronic angular momentum projection quantum number, which may take on any integer value. Within this extended basis set, the electronic operators $|x\rangle\langle x| - |y\rangle\langle y|$ and $|x\rangle\langle y| + |y\rangle\langle x|$ in the Hamiltonian on the second line of eq 4 may be regarded as restrictions of 2 $\cos(2\theta)$ and -2 $\sin(2\theta)$, respectively. Taking $q_1 = \rho\cos\phi$ and $q_2 = \rho\sin\phi$, where ρ and ϕ are the standard coordinates for an isotropic two-dimensional harmonic oscillator,[45] the Longuet-Higgins extended Hamiltonian thus has a vibrational-electronic interaction (second line of eq 4) given by

$$\hat{\mathbf{H}}_{ev} = 2\omega d\hat{\rho}\cos(2\hat{\theta} - \hat{\phi}) \tag{6}$$

Taking q_1 and q_2 as the standard b_{1g} and b_{2g} normal modes for a square symmetric molecule,[37] a positive displacement d in eq 4 gives the Jahn–Teller effect on a particle in a square 2D box[46−48] expected from the Hellmann–Feynman theorem.[49]

The extended Hamiltonian does not depend on the pseudorotation angle $\phi + (\theta/2)$ orthogonal to $2\theta - \phi$. The cyclic coordinate[50,51] $\phi + (\theta/2)$ thus gives rise to a conserved pseudorotation quantum number $j = l + (\lambda/2)$ where l is the quantum number for the vibrational angular momentum conjugate to ϕ (any multiple of j is conserved). Since l is an integer and $\lambda = \pm 1$, this pseudorotation quantum number j has been chosen half-odd-integral,[8] a choice motivated by the appearance of the eigenfunctions below. j is a signed quantum number with complex-valued eigenstates, all energy levels are doubly degenerate with respect to the sign of j.

For the computations presented in this paper, we use a direct product of one-dimensional harmonic oscillator vibrational basis states in the dimensionless normal coordinates q_1 and q_2. The 1D harmonic oscillator matrix elements are also chosen to follow the phase convention in ref 45, which assumes that the rightmost lobe at positive q always has positive amplitude. With this phase convention, the complex-valued isotropic two-dimensional harmonic oscillator basis states obey $\sigma_v|v, l\rangle = |v, -l\rangle$.[52] This is consistent with the phase convention of Condon and Shortley and electronic angular momentum projection basis states that obey $\sigma_v|\lambda\rangle = |-\lambda\rangle$.[53] (This phase convention differs from those of Moffitt and Liehr[4]

DOI: 10.1021/acs.jpca.7b07140
J. Phys. Chem. A 2017, 121, 7401−7413

Table 1. Six Lowest Energy Eigenvalues for Small Jahn-Teller Stabilization Energies with ω = 200 cm^{-1}

					$(D\omega)$ [cm^{-1}]			
v	$\lvert j\rvert$	l	λ	$E^{(2)}$	0.01	0.1	1	5
0	1/2	0	±1	$\omega - 2(D\omega)$	199.980	199.800	198.010	190.235
1	3/2	±1	±1	$2\omega - 4(D\omega)$	399.960	399.601	396.058	381.292
1	1/2	±1	∓1	2ω	400.000	400.000	399.980	399.516
2	5/2	±2	±1	$3\omega - 6(D\omega)$	599.940	599.401	594.143	572.999
2	1/2	0	±1	$3\omega - 2(D\omega)$	599.980	599.800	598.030	590.718
2	3/2	±2	∓1	$3\omega + 2(D\omega)$	600.020	600.199	601.912	607.918

and of Oka.[44]) Together, these establish that degenerate energy eigenstates of the pseudorotation quantum number may be found from the corresponding pair of degenerate σ_v eigenstates as $|m, \pm j\rangle = (|m,+\rangle \pm i|m,-\rangle)/2^{1/2}$. Such complex-valued eigenstates exhibit the circular symmetry of the Hamiltonian.

For Jahn−Teller stabilization energies that are small relative to the vibrational frequency, second-order perturbation theory[44] leads to the following expression for the energies

$$E^{(2)}_{v,j} = \omega(v + 1) - 2(D\omega)[l\lambda + 1] \quad (7)$$

In eq 7, the vibrational quantum number v and the pseudorotation quantum number j on the left combine to unambiguously determine the relative signs of the vibrational (l) and electronic (λ) angular momentum quantum numbers on the right. Since l = v, (v − 2)... − v and λ= ± 1, a given $j = l + (\lambda/2)$ can only arise in one way for each v. Equation 7 contains an isotropic 2D harmonic oscillator energy ω(v + 1), Jahn−Teller stabilization along both coordinates $[-2(D\omega)]$, and a typical internal angular momentum coupling[54] contribution to the energy $[-2(D\omega)l\lambda]$. Equation 7 shows that the energy depends on the relative sign of l and λ, not their individual signs. The form of this last term can be expected based on the analogy to vibrational-vibrational angular momentum coupling discussed by Oka.[44]

COMPUTATIONAL METHODS

Computations use a basis state approach to enable high local resolution in the vibrational coordinates for study of the nodes. States are calculated using a truncated vibronic Hamiltonian matrix that includes n one-dimensional harmonic oscillator basis states for each coordinate, so that there are n^2 vibrational basis states on each of the two diabatic electronic basis states. Diagonalizing this Hamiltonian matrix yields $2n^2$ nonadiabatic eigenstates. The harmonic oscillator basis states are all centered at the origin. Off-diagonal matrix elements in dimensionless normal coordinates are calculated analytically.[45] The truncated Hamiltonian is numerically diagonalized using the DEVCSF routine from the IMSL library,[55] which calculates eigenvectors and eigenvalues using an implicit QR algorithm[56] (which does not respect other symmetries in the Hamiltonian). Four steps are taken to generate unique eigenstate symmetries and phases. First, a numerically stable basis set rotation for σ_d symmetry[32] is applied to each pair of degenerate eigenvectors before sorting into σ_d eigenvalues of +1 and −1. Second, each pair of degenerate states is then basis-set-rotated by $\pi/4$ to generate σ_v symmetry states,[32] which are sorted into states with eigenvalues of +1 and −1. Third, for each σ_v eigenstate, the overall sign is then changed, if necessary, to make the basis state coefficient with the largest magnitude positive [so states have dominant + $|x\rangle$ or + $|y\rangle$ electronic character]. Fourth, for each σ_d eigenstate, the overall sign is changed, if necessary, to make the largest magnitude basis state coefficient on x positive [so states have dominant $(|x\rangle + |y\rangle)/2^{1/2}$ or $(|x\rangle - |y\rangle)/2^{1/2}$ electronic character]. In cases where these rules decide the sign based on finite numerical precision, sign adjustments are made for consistency between figures.

For a vibrational frequency of 200 cm^{-1} and a reorganization energy of 10 cm^{-1}, increasing the number of harmonic oscillator basis states for each vibration from 13 to 25 (from a total of 338 to a total of 1250 vibronic states) indicates that the 12 lowest eigenvalues are all converged to within 2×10^{-12} cm^{-1} and that all of their 338 common normalized basis state coefficients are converged to within 4.3×10^{-10}. Higher energy states or larger stabilization energies can require a larger basis to establish convergence (see the Supporting Information). The lowest 12 eigenvalue pairs are degenerate beyond the 14th digit (to within 2×10^{-12} cm^{-1}). With the basis states used, eigenstates of σ_v have a systematic pattern of zeros in their coefficients;[32] all coefficients that should be zero by symmetry have magnitudes of less than 2×10^{-14}. Using a basis of 25 normalized harmonic oscillator eigenfunctions for each coordinate on a discrete 2D grid with 0.01 spacing over the domain [−9,9], the 12 lowest two-dimensional eigenfunctions are orthogonal to within 4.8×10^{-14} and normalized to within 2.2×10^{-12}. The normalized eigenfunctions are converged at all grid points to within 10^{-14}.

For several Jahn−Teller stabilization energies, Table 1 gives the quantum numbers and numerical energy eigenvalues for the six lowest energy levels. Dominant basis state quantum numbers and second order perturbation theory expressions for the energies from eq 7 are in the columns at left. Each energy level is doubly degenerate, so these levels correspond to the 12 lowest eigenstates.

The nonadiabatic energies in Table 1 demonstrate that perturbation theory is quantitatively accurate for small Jahn−Teller stabilization energies $[(D\omega) \ll \omega]$, smaller vibrational quantum numbers v, and smaller magnitude pseudorotation quantum numbers $|j|$. The Supporting Information contains a more extensive table with more states, a larger range of Jahn−Teller stabilization energies, and more accurate energies. The energies there quantitatively reproduce those reported by Longuet-Higgins et al.[5] for pseudorotation quantum numbers j = 1/2 and 3/2, all of which involve larger displacements than in Table 1.

RESULTS

Figure 2 provides a complete characterization of the 12 lowest nonadiabatic eigenfunctions for a "submerged" conical intersection that is well below the zero point energy. These 12 eigenfunctions occur in degenerate pairs for the 6 lowest energy levels in Table 1. The exact factorization is used to show a positive amplitude and color is used to show the electronic character, including all phase/sign information. At each point in

DOI: 10.1021/acs.jpca.7b07140
J. Phys. Chem. A 2017, 121, 7401−7413

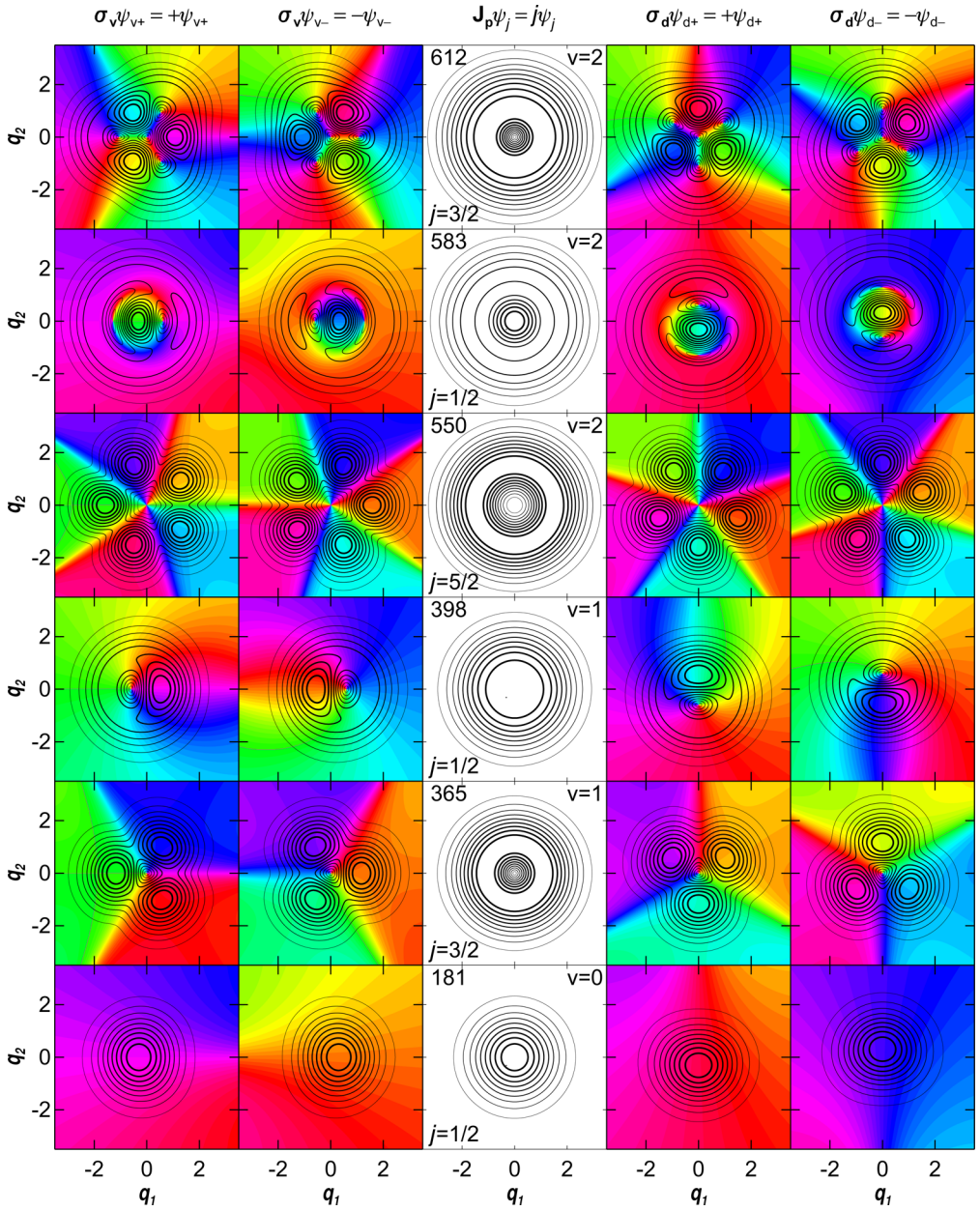

Figure 2. Three representations of the lowest 12 nonadiabatic eigenstates of the Hamiltonian with Jahn−Teller stabilization energy $(D\omega)$ = 10 cm^{-1} and vibrational frequency ω = 200 cm^{-1}. The contours indicate the nonadiabatic amplitude factor $P_m(q_1,q_2)$ and the colors (in columns 1, 2, 4, and 5) indicate the nonadiabatic electronic character $|K_m(q_1,q_2)\rangle$ using the color wheel in Figure 1. Together, these factors fully characterize real-valued nonadiabatic eigenfunctions. For each eigenstate, the contours are at multiples of 10% of the maximum amplitude, with higher contour lines being thicker. Because of the pairwise exact degeneracy, these states have been further specified using three noncommuting operators that each commute with the Hamiltonian. The first two columns show real-valued eigenstates of the σ_v operator with eigenvalues of +1 and −1, respectively. These two columns contain the complete set of the lowest 12 eigenstates. The middle column shows the circularly symmetric amplitude factor for complex-valued eigenstates with a signed pseudorotation quantum number j. In this column, each panel also gives the vibrational quantum number v and the energy in wavenumbers (cm^{-1}) for its row. The fourth and fifth columns show the same complete set of the 12 lowest eigenstates as real-valued eigenstates of σ_d, with eigenvalues of +1 and −1, respectively.

the vibrational coordinate space, the electronic character and phase are displayed as an electronic angle using eq 3. As in ref 26, isolated point nodes in the amplitude factor are always accompanied by singularities in the electronic factor. The total nonadiabatic eigenfunctions are single-valued and continuously differentiable, *apparent* derivative discontinuities in the vibrational amplitude on crossing through a vibrational node are compensated by an electronic sign change at the electronic singularity. The leftmost two columns show real-valued degenerate eigenstates of σ_v, the rightmost two columns show the real-valued linear combinations of these same two states that are eigenfunctions of σ_d, and the middle column shows the magnitude for either complex-valued linear combination of these same two states with a signed pseudorotation quantum number. The circular symmetry of the conical intersection is reflected in the circularly symmetric magnitudes of the complex-valued eigenstates with signed pseudorotation quantum numbers. With respect to the sign of j, these

DOI: 10.1021/acs.jpca.7b07140
J. Phys. Chem. A 2017, 121, 7401−7413

eigenfunctions occur in degenerate pairs, but the real and positive amplitude factor is independent of the sign of j and the complex-valued electronic character is not shown (it would require a different color wheel), so a single column suffices. Precursors of half-odd-integral adiabatic pseudorotation are already visible in the 3-fold and 5-fold symmetric vibrational amplitude factors P_m for the real-valued eigenfunctions with $|j| = 3/2$ and $|j| = 5/2$, respectively.

At the same time, the adiabatic electronic sign change (Berry phase of $\pm\pi$) required for a path circling the conical intersection (see Figure 1) does not appear for the exact total eigenfunctions in Figure 2. As noted by Longuet-Higgins et al.,[5] an adiabatic sign change in the electronic factor must be compensated by a sign change in the nuclear factor so that their product is an overall single-valued total wave function. The single-valued total eigenfunctions in Figure 2 are not confined to a single adiabatic surface and are far from the adiabatic limit. Around the conical intersection, each nonadiabatic eigenfunction makes an integer number of circuits around the electronic color wheel (as required by continuity).

The v = 0, $j = 1/2$ zero point eigenstates and higher $j = 1/2$ states in Figure 2 all have nonzero amplitude at the origin, where the conical intersection is located. The higher $|j| = 1/2$ states have "accidental" conical nodes in different locations for σ_v and σ_d eigenstates. These disappear for circularly symmetric pseudorotation eigenstates. For example, in Figure 2, v = 1, $|j| = 1/2$ and v = 2, $|j| = 1/2$ have 1 and 2 accidental conical nodes, respectively. These "accidental" conical nodes arise in the same way as the "accidental" conical nodes in ref 26.

All $|j| = 3/2$ states have 3-fold symmetry in the amplitude factor $P_m(q_1,q_2)$ and "essential" conical nodes at the conical intersection. We call these nodes essential because they occur at the same location for eigenstates of all three noncommuting operators. For all essential nodes, the absolute numerical eigenfunction amplitudes at the origin are less than 2×10^{-14}. In addition to the essential conical node, the higher $|j| = 3/2$ states have accidental conical nodes away from the origin; v = 2, $|j| = 3/2$ in Figure 2 has three accidental conical nodes. Circling each conical node by itself, the electronic character makes one circuit around the color wheel.

The essential node at the origin of the 5-fold symmetric amplitude $P_m(q_1,q_2)$ for v = 2, $|j| = 5/2$ is not conical, as can be seen from the contour spacings. For this single node, the electronic character makes two circuits around the color wheel. These properties are connected and will be explored below after investigating the $|j| = 1/2$ levels.

For the zero point level and all states with pseudorotation quantum number $|j| = 1/2$, Figure 2 shows nonzero probability amplitude on top of the conical intersection at the origin. Furthermore, the maximum probability amplitude is off-center for the real-valued eigenfunctions. Table 1 shows that the perturbation theory errors in energy are small for the zero point level. Therefore, perturbation theory should be useful for understanding the off-center maximum in the zero point probability density indicated by Figure 2.

Figure 3 shows the zero point eigenstate's exact factorization and its projections onto the diabatic basis states for Jahn–Teller stabilization energies of $(D\omega) = 5$ cm^{-1} and $(D\omega) = 20$ cm^{-1}. In first-order perturbation theory, the zero-point basis state with $\sigma_v = +1$ becomes

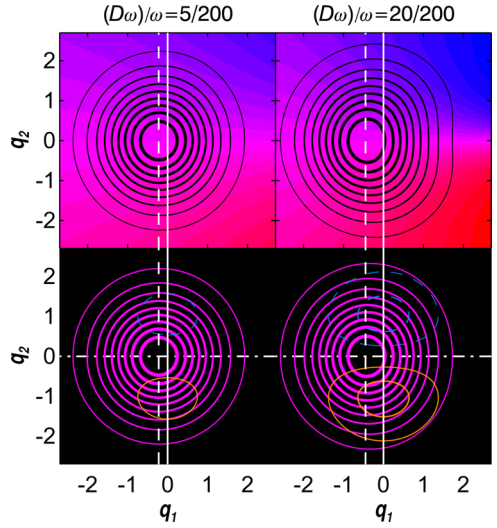

Figure 3. Exact factorization (top row) and coordinate-dependent projections of zero-point eigenstates with $\sigma_v = +1$ onto the diabatic electronic basis states (bottom row) for two different Jahn–Teller stabilization energies $(D\omega)$ with vibrational frequency $\omega = 200$ cm^{-1}. The factorization is plotted as in Figure 2. Both diabatic projections are overlaid using the color wheel in Figure 1. Positive projections $\langle q_1,q_2\langle x|\psi_0\rangle$ have solid magenta contours at 10% of P_{max}. Projections $\langle q_1,q_2\langle y|\psi_m\rangle$ have solid orange 10% contours when positive, dashed blue 10% contours when negative, and a dot-dashed white line marking the node. The solid white vertical lines mark $q_1 = 0$. The dashed white vertical lines mark $q_1 = -d$, the equilibrium vibrational displacement of $|x\rangle$. (Left column) $(D\omega) = 5$ cm^{-1} [$d = (1/20)^{1/2} \approx 0.2236$]. (Right column) $(D\omega) = 20$ cm^{-1} [$d = (1/5)^{1/2} \approx 0.4472$].

$$\left|\psi^{(1)}_{0,0,x}\right\rangle = |v_1 = 0,\ v_2 = 0\rangle|x\rangle - (d/2^{1/2})|v_1 = 1,\ v_2 = 0\rangle|x\rangle - (d/2^{1/2})|v_1 = 0,\ v_2 = 1\rangle|y\rangle \quad (8)$$

In eq 8, all one-dimensional harmonic oscillator basis states are centered on the origin. For $(D\omega) = 5$ cm^{-1}, normalizing this approximation yields projections that are visually indistinguishable from the exact projections at the scale shown.[57] The crucial insight from Figure 3 is that the off-center maximum occurs at $(q_1,q_2) = (-d,0)$ for the $\sigma_v = +1$ eigenstate. Quantitatively, the maxima in Figure 3 occur at −0.220 (for $d = 0.224$) and −0.425 (for $d = 0.447$); the position of the maximum approaches $-d$ quantitatively as d decreases, exceeding three digit accuracy for $d = 0.1$. Perturbation theory also correctly indicates that the off-center maximum occurs at $(+d,0)$ for the $\sigma_v = -1$ zero point eigenstate, $(0,-d)$ for $\sigma_d = +1$, and $(0,+d)$ for $\sigma_d = -1$. The real-valued zero point eigenstates are driven off-center by the Jahn–Teller stabilization energy and have their maximum probability density near the equilibrium displacement of their dominant electronic basis state (so long as that displacement is small).

For this high symmetry model, the location and number of the "accidental" conical nodes are not truly accidental. For example, the accidental nodes for $j = 3/2$ states occur in sets of 3 at a common radius and have predictable angles for each reflection symmetry. Similarly, the higher $j = 1/2$ states with vibrational quantum number v have v accidental conical nodes. These nodes occur along the q_1 axis for σ_v eigenstates and along the q_2 axis for σ_d eigenstates. Using the reflection symmetry dependent equilibrium displacements found in the discussion

DOI: 10.1021/acs.jpca.7b07140
J. Phys. Chem. A 2017, 121, 7401−7413

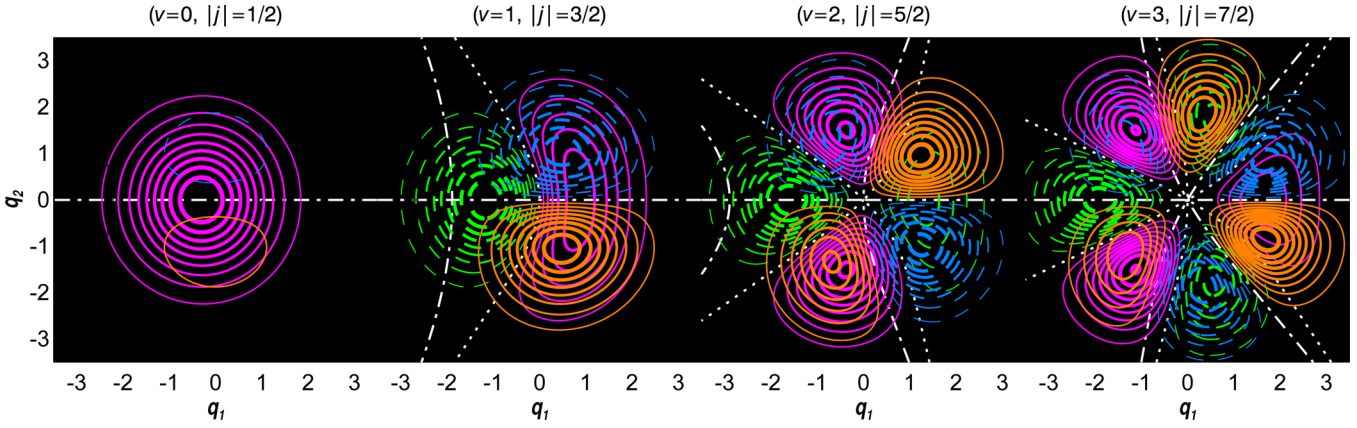

Figure 4. Coordinate dependent projections of 4 nonadiabatic eigenstates onto the diabatic electronic basis states, all shown as eigenstates of σ_v with eigenvalue +1. Using the color wheel in Figure 1, projections $\langle q_1,q_2\langle x|\psi_m\rangle$ have solid magenta contours when positive and dashed green contours when negative, with white dotted lines marking zero. Each projection is overlaid with the corresponding projection $\langle q_1,q_2\langle y|\psi_m\rangle$ which is solid orange when positive, dashed blue when negative, and dot-dashed white when zero.

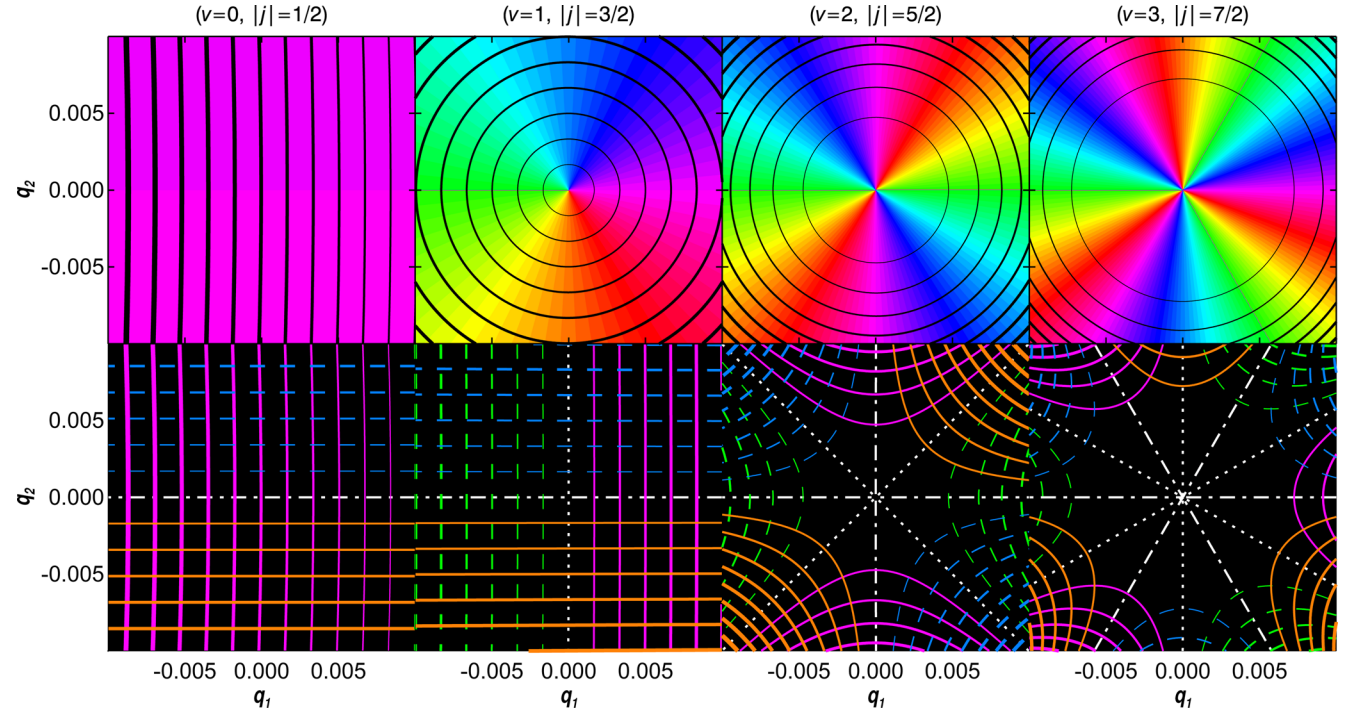

Figure 5. Close up view around the origin for the σ_v = +1 eigenstates in Figure 4. (Top row) Exact factorization with positive contours for the amplitude factor $P_m(q_1,q_2)$ and color for the electronic character $|K_m(q_1,q_2)\rangle$ using the color wheel in Figure 1. (Bottom row) Overlaid coordinate dependent projections onto the electronic basis states $\langle q_1,q_2\langle x|\psi_m\rangle$ (using solid magenta contours for positive amplitude, dashed green contours for negative amplitude, and dotted white curves for zero) and $\langle q_1,q_2\langle y|\psi_m\rangle$ (using solid orange contours for positive amplitude, dashed blue contours for negative amplitude, and dot-dashed white curves for zero). The contour levels change from panel to panel. (v = 0, |j| = 1/2) in the leftmost column has no node, and the exact factorization contours are at 0.05% intervals from 95.15% to 95.65%, the *x*-projection contours are at 0.05% intervals from 95.15% to 95.65% of P_{max}, and the *y*-projection contours are at 0.05% intervals of P_{max} around 0. (v = 1, |j| = 3/2) has a conical node, and the contour intervals are 0.2% of P_{max} for the exact factorization and the projections. (v = 2, |j| = 5/2) has a quadratic node and contour intervals of 2×10^{-5} P_{max}. (v = 3, |j| = 7/2) in the rightmost column has a cubic node and contour intervals of 2×10^{-7} P_{max}.

of the zero point states above, the locations approximate the zeroes of displaced one-dimensional harmonic oscillator eigenfunctions with v_1 = v (for σ_v eigenstates) and v_2 = v (for σ_d eigenstates). The higher states (see the Supporting Information) reveal more systematic patterns. The number of accidental axial and radial node distances is (v − |j| + 1/2) and each radial node distance has 2|j| nodes, so that the total number of accidental nodes is 2|j|(v − |j| + 1/2). (This result has limited generality because the isotropic 2D harmonic oscillator quantum number v goes bad in the adiabatic limit.) For the same reasons stated in ref 26, these accidental nodes have the shape of right elliptical cones with the node at the vertex. For every state examined, their principal axes are observed to be radial and angular, with the minor axis in the radial direction. In short, the "accidental" conical nodes are consequences of the circular symmetry of the model.

Figure 4 shows the projections of 4 nonadiabatic eigenfunctions onto the diabatic electronic basis states. Nodes

DOI: 10.1021/acs.jpca.7b07140
J. Phys. Chem. A 2017, 121, 7401−7413

in each projection are shown as dotted and dot-dashed white lines. When two white lines from different projections cross, the amplitude on both basis states must be zero so that the nonadiabatic eigenfunction must have a node; this occurs only at the origin for these states. Figure 4 illuminates how half-odd-integer avoided angular nodes arise from integer angular nodes in the underlying projections. The lowest states with j = 3/2, 5/2, and 7/2 have 1, 2, and 3 angular nodes through the origin in each projection, respectively, giving a total of 4, 8, and 12 angular half nodes over both projections. In each case, half of an angular node along the negative q_1 axis disappears under a negative minimum in the x projection. This leaves 3 angular half nodes for j = 3/2, which all become avoided half nodes. For j = 5/2 and 7/2, angular node halves curve close together in 2 and 4 pairs, respectively, to reduce the number of angular avoided half nodes to 5 and 7. Figure 5 zooms in to reveal the nodal behavior near the origin.

Figure 5 shows how, for increasing values of the pseudorotation quantum number, the essential nodes at the origin have an increasing order. In the exact factorization (top panels), this order can be easily characterized by the number of rotations around the electronic color wheel. The order can also be characterized by the radial spacing of the contours, which are evenly spaced in amplitude for each panel. From left to right: v = 0, j = 1/2 has no node and the electronic character does not circle the color wheel (0th order): v = 1, j = 3/2 has a right circular conical node with its vertex at the origin, the even spacing of contours with radius indicates a linear amplitude proportional to ρ and the electronic factor makes one circuit around the electronic color wheel, so this is a first order node; for v = 2, j = 5/2, the growth in contour spacing with radius quantitatively indicates a quadratic amplitude proportional to ρ^2 and the electronic factor makes two circuits around the color wheel, so this is a second order node; for (v = 3, j = 7/2), the contours have a cubic amplitude growing as ρ^3 for small ρ and the electronic factor makes three circuits around the color wheel, so this is a third order node. The coordinate dependent projections of the eigenstates onto diabatic basis states in the bottom panels provide insight into these orders. Except for the j = 1/2 state, the number of angular nodes in each projection matches the order. At the conical node in (v = 1, j = 3/2), one nodal line on $|x\rangle$ intersects one nodal line on $|y\rangle$. At the quadratic node in (v = 2, j = 5/2), two nodal lines on $|x\rangle$ and two nodal lines on $|y\rangle$ all intersect. For the cubic node in (v = 3, j = 7/2), there are three nodal lines on each state that all converge on the origin. The essential nodes at the conical intersection are consequences of circular symmetry, for which higher vibrational angular momentum requires higher radial powers in the amplitude.

In Figure 5, higher order nodes at the conical intersection exhibit a link between the radial exponent for the vibrational amplitude factor and the number of circuits around the electronic color wheel at small ρ, both are given by $|j| - 1/2$, where j is the pseudorotation quantum number. This linkage can be proven based on a conserved pseudorotation quantum number. With a conserved pseudorotation quantum number and electronic angular momentum projection quantum numbers of $\lambda = \pm 1$, an eigenstate with a given signed $j = l + (\lambda/2)$ can have contributions from basis states with only two signed vibrational angular momentum quantum numbers, $l = j \pm (1/2)$. Thus, $|l|_{min} = |j| - (1/2)$. Around the origin, the local behavior of the eigenstates for the isotropic two-dimensional harmonic oscillator is given by the power series term of lowest order, which is proportional to $\rho^{|l|} \exp(il\phi)$. The two degenerate eigenstates have lowest order terms proportional to

$$\psi_{v,j}(\rho, \phi) \sim \rho^{|l|_{min}} \exp(\pm i|l|_{min}\phi)[|x\rangle \pm i|y\rangle]/2^{1/2} \quad (9)$$

In eq 9, the symbol $\sim$ means leading order proportionality in the limit as $\rho \to 0$. Equation 9 proves that essential nodes have true zeros in eigenfunction amplitude at the conical intersection. Linear combinations can give real-valued eigenfunctions with a local behavior of

$$\psi_{v,|j|}(\rho, \phi) \sim \rho^{|l|_{min}} \cos(|l|_{min}\phi - \alpha)|x\rangle - \rho^{|l|_{min}} \sin(|l|_{min}\phi - \alpha)|y\rangle \quad (10a)$$

and

$$\psi_{v,|j|}(\rho, \phi) \sim \rho^{|l|_{min}} \sin(|l|_{min}\phi - \alpha)|x\rangle + \rho^{|l|_{min}} \cos(|l|_{min}\phi - \alpha)|y\rangle \quad (10b)$$

where α is an arbitrary reflection symmetry plane angle. The σ_v eigenstates have $\alpha = 0$, and the σ_d eigenstates have $\alpha = \pi/4$. The $\sigma_v = +1$ [$\sigma_v = -1$] eigenfunctions in Figure 2 follow eq 10a [eq 10b] with $\alpha = 0$ and $|l|_{min} = |j| - 1/2$. Inserting eq 10 into eqs 1−3 gives

$$\text{Þ}_{v,|j|}(\rho,\phi) \sim \rho^{|l|_{min}} \quad (11)$$

and

$$\Theta_{v,|j|}(\rho, \phi) \sim -(|l|_{min}\phi - \alpha) \quad (12a)$$

for the $\sigma_v = +1$ eigenfunctions in eq 10a or

$$\Theta_{v,|j|}(\rho, \phi) \sim -(|l|_{min}\phi - \alpha) + \pi/2 \quad (12b)$$

for the $\sigma_v = -1$ eigenfunctions in eq 10b.

We now define the "electronic index" $\eta(C)$ through a line integral around any simple closed counterclockwise path C that does not pass through a node,

$$\eta(C) = \frac{1}{2\pi} \oint_C d\Theta_m(q_1, q_2) \quad (13)$$

In pictorial terms, the electronic index is equal to the number of counterclockwise spins around the color wheel on the path of integration. With this definition, the electronic index is independent of the arbitrary overall sign of the eigenfunction [by the definition of Θ_m in eq 3] and the arbitrary phase α but does depend on the phase convention for the electronic basis states $|x\rangle$ and $|y\rangle$. In other words, electronic indices are significant relative to each other, even for different eigenstates. Since the nonadiabatic eigenfunctions are real-valued, continuous, and differentiable, they form a differentiable vector field (see ref 58) of electronic state vectors over the vibrational coordinates (this is why Θ_m is defined in terms of ψ_m). The electronic index is the index of this vector field over the oriented planar surface of vibrational coordinates. This has two consequences: first, the electronic index is an integer (a result also required by single-valued wave function continuity); second, the electronic index depends only on the number, order, and sign of the nonadiabatic nodes enclosed by the path (a new result). The electronic indices for paths that circle only the essential node at the conical intersection can be obtained from eqs 12 and 13 using a path at small constant radius so that

DOI: 10.1021/acs.jpca.7b07140
J. Phys. Chem. A 2017, 121, 7401−7413

$d\Theta_{v,|j|}(\rho, \phi) = -|l|_{min} d\phi$ and $\eta(C) = -|l|_{min}$ or by visual inspection of Figure 2. The electronic indices around the conical intersection are $\eta(C) = 0$ for (v = 0, |j| = 1/2), $\eta(C) = -1$ for (v = 1, |j|= 3/2), $\eta(C) = 0$ for (v = 1, |j| = 1/2), $\eta(C) = -2$ for (v = 2, |j| = 5/2), $\eta(C) = 0$ for (v = 2, |j| = 1/2), and $\eta(C) = -1$ for (v = 2, |j| = 3/2).

Locally, the vibrational radial exponent and the electronic index have precisely the same magnitude and define the order of the essential node as $|l|_{min} = |j| - 1/2$. Furthermore, the sign of the electronic index for a sufficiently small loop around the origin is the same for all essential nodes. Remarkably, the essential node signs are all opposite the sign of the conical intersection, which is defined by the sign of the counterclockwise line integral around the conical intersection:

$$\gamma(C) = \frac{1}{2\pi} \int_C d\Theta^a(q_1, q_2) \tag{14}$$

In eq 14, Θ^a is the adiabatic electronic mixing angle. [$2\pi\gamma(C)$ has been called the Longuet-Higgins phase[59] and is an integer multiple of π for two real-valued electronic states. When 3 electronic states are involved, the geometric phase defined through the nonadiabatic derivative coupling[6,60] has been reported to differ from exact integer multiples of π,[61] but it converges to the Longuet-Higgins phase for infinitesimal loops.[59−61]] The line integral can either start and stop at the discontinuity for a single-valued Θ^a or be closed for a double-valued Θ^a (half-integer line integrals are possible because the adiabatic electronic eigenfunctions do not form a *differentiable* vector field over an oriented surface). The sign of a conical intersection, sgn(γ), has the same dependence on the phase convention for the electronic basis set as the electronic index (and no dependence on arbitrary adiabatic eigenfunction sign or phase). The line integral around the conical intersection in Figure 1 is $\gamma(C) = +1/2$, so the sign of the conical intersection is positive; it is independent of which adiabatic surface (upper or lower) is used to evaluate it. As a result, the sign of a conical intersection is meaningful relative to the electronic indices for all nodes. The sign of the conical intersection can be reversed by reversing the sign of the Jahn−Teller displacement d in either the diagonal or off-diagonal Jahn−Teller coupling term in the Hamiltonian. Figure 6 shows the adiabatic surfaces and the lowest energy 6 nonadiabatic eigenstates of σ_v for a conical intersection with a negative sign generated by reversing the sign of the diagonal coupling. All of the equilibrium displacements along q_1 are reversed with respect to Figure 2, and all of the conical node signs are reversed.

In contrast to a submerged conical intersection, a high energy conical intersection will push the amplitude away from the origin on the lower surface. In the isotropic 2D harmonic oscillator basis, this involves cancellation of the lowest order radial powers between basis states with the same vibrational angular momentum l but different vibrational quantum numbers v [for example, cancellation of the constant radial term between (v = 0, l = 0) and (v = 2, l = 0)]. Thus, $|j| - 1/2$ is a *lower bound* on the radial power law exponent for the vibrational amplitude near the origin. For adiabatic eigenfunctions confined to the lower surface, which require a high conical intersection, various models indicate that the lowest radial power law exponent must exceed $\sqrt{1/2}$ (ref 62), $(1/2) + \sqrt{1/2}$ (ref 63) or $\sqrt{5/2}$ (ref 64).

This proves that, near the origin, all eigenstates of the circular symmetry conical intersection have a vibrational amplitude factor with a radial power law exponent of *at least* $|j| - 1/2$ and an electronic factor that circles the electronic color wheel *exactly* $|\eta(C)| = |j| - 1/2$ times. This allows states with $|j| = 1/2$ to have nonzero amplitude at the conical intersection, proves

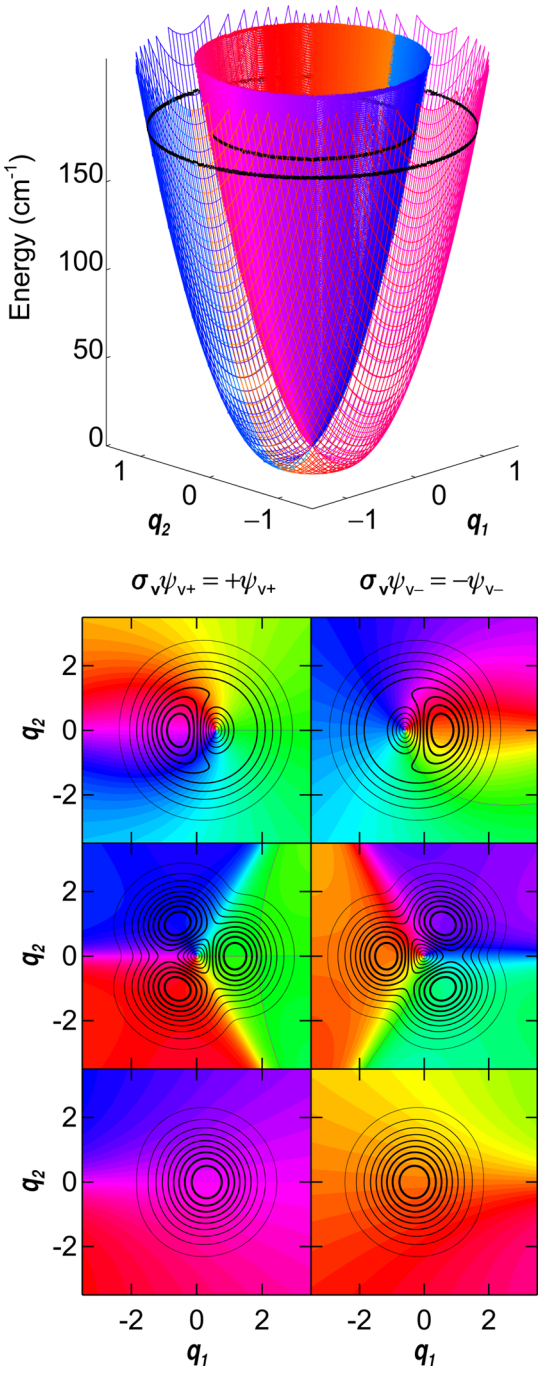

Figure 6. (Top) Adiabatic potential energy surfaces and coordinate dependent electronic character for a model Hamiltonian in which the sign of the Jahn−Teller displacement along q_1 has been reversed compared to Figure 1. All other parameters are the same as in Figure 1. In contrast to Figure 1, a counterclockwise path around either adiabatic surface now rotates halfway around the color wheel in a clockwise direction. (Bottom) The 6 lowest energy real-valued eigenstates of σ_v with reversed displacement along q_1. All other parameters are the same as in Figure 2. For each eigenstate, the sense of rotation around the color wheel is reversed in comparison to the corresponding eigenstate in Figure 2.

DOI: 10.1021/acs.jpca.7b07140
J. Phys. Chem. A 2017, 121, 7401−7413

that states with $|j|$ = 3/2 can have conical nodes with the form of a right circular cone at the conical intersection, and establishes the linked vibrational-electronic form of the higher order nodes at the conical intersection. Circular symmetry was assumed for the above proof; the results may not apply for lower symmetry conical intersections.

It was proven above that the essential nodes at the conical intersection all have the same sign for the local electronic index. The accidental conical nodes do not. For example, the (v = 2, $|j|$ = 1/2) states in Figure 2 have two oppositely signed nodes, such that the electronic index is zero for any path that encompasses them both. All of the conical nodes in ref 26 occur in such oppositely signed pairs. However, any counterclockwise circuit that encompasses all 4 conical nodes in (v = 2, $|j|$ = 3/2) has an electronic index of $\eta(C)$ = +2. This addition of electronic indices for the 4 conical nodes is precisely analogous to the addition of geometric phase line integrals for the 4 conical intersections in the linear plus quadratic $E\otimes e$ C_{3v} Jahn−Teller coupling treated by Zwanziger and Grant.[17] Here, it arises because the conical node at the origin has an electronic index of −1 while the three accidental conical nodes have electronic indices of +1, so that the sum of the enclosed electronic indices is +2. Note that this eigenstate has $l = \pm 2$ and $\lambda = \mp 1$, so that $\lambda l = -2$. For every state examined (all states through v = 4), the signed large radius electronic index is equal in magnitude and opposite in sign to $\lambda l\ \mathrm{sgn}(\gamma)$, where $\mathrm{sgn}(\gamma)$ is the sign of the conical intersection [$\mathrm{sgn}(\gamma)$ = +1 in Figure 1]; this is proportional to the electronic-vibrational angular momentum coupling term in the second-order perturbation theory eigenstate energies of eq 7.

DISCUSSION

The results obtained here directly address questions about wave function amplitude around conical intersections. Mead has shown that single-surface eigenfunctions must approach zero at a conical intersection in two-dimensions.[62] Varandas and Xu have provided analytic support for this result in X_3 molecules.[64] For a pure conical intersection potential, Yarkony found that the eigenfunctions approach zero at the conical intersection.[63] The above treatments do not directly address systems for which the conical intersection is weak or submerged.

Weak or submerged conical intersections are, as mentioned in the Introduction, common in molecular Jahn−Teller distortions. In such circumstances, nonadiabatic eigenfunctions can span more than one adiabatic surface, as in the pioneering study by Moffitt and Liehr.[4] Although a different basis and phase convention are used, the perturbation theory results of Moffitt and Liehr [their eqs 36 and 38] are equivalent to eq 8. For the zero point level, these expressions place large amplitude at the conical intersection, and this amplitude is continuously present with the same sign as the Jahn−Teller displacement d is tuned through 0 (where the zero point eigenfunction becomes the zero point level for an isotropic two-dimensional harmonic oscillator, which guarantees a nonzero amplitude on the conical intersection). This example (which is 60 years old) thus concretely illustrates nonzero nonadiabatic eigenfunction amplitude at a conical intersection, a phenomenon discussed in refs 33 and 23.

The large wave function amplitude at the origin for low energy eigenstates of a submerged conical intersection with circular symmetry suggests similar amplitude at the submerged lower symmetry D_{4h} conical intersection for the silicon naphthalocyanine studied in refs 30−32. This actual sampling of the high symmetry geometry contrasts with the high symmetry average geometry produced by interconversion among equivalent low symmetry geometries[18] (often while *avoiding* the high symmetry geometry[19]) in the dynamical Jahn−Teller effect. Evidently, nonzero wave function amplitude at the high symmetry geometry may be anticipated for the ground vibrational state in many molecules with weak dynamical Jahn−Teller effects.

As the analysis of Figure 3 shows, the zero-point state's maximum amplitude follows the Jahn−Teller displacement away from the conical intersection. Thus, even with the highest possible Jahn−Teller symmetry, the average geometry of one degenerate eigenstate is not necessarily the undistorted high symmetry geometry (though averaging over both degenerate eigenstates always restores the high symmetry). As the Jahn−Teller stabilization energy increases, these nonadiabatic results are apparently heading toward agreement with the adiabatic results for a conical intersection with sufficiently high energy to confine low energy eigenstates onto the lower adiabatic surface. However, to form a complete basis, some eigenstates with sufficiently high energy must have eigenfunction amplitude in an arbitrarily small region around the conical intersection.

Figure 7 shows how the nonadiabatic eigenfunctions for v = 1, $|j|$ = 3/2 begin approaching the limit of adiabatic pseudorotation. For small Jahn−Teller stabilization energy, there is a conical node at the origin and three strongly avoided angular half nodes. These nonadiabatic eigenfunctions are everywhere single-valued and continuous, with continuous derivatives, the apparent derivative discontinuities in the amplitude crossing through the origin are compensated by the electronic sign change. Their 2π angular periodicity corresponds to the adiabatic product of compensating electronic and vibrational factors with half-odd-integral angular momenta,[5,43] so the Longuet-Higgins phase is hidden. As the height of the conical intersection increases, the conical node at the origin starts to connect three weakly avoided angular half nodes that will become the three angular half nodes in the adiabatic limit. In the projections onto the diabatic states, the incipient formation of adiabatic nodes is associated with the dotted nodal curve on $|x\rangle$ that is moving in from the right. Forming true angular half-nodes for the adiabatic limit will require that this nodal curve on $|x\rangle$ precisely coincide with the nodal curve on $|y\rangle$ (dot-dashed). Until this additional node coincides exactly, the derivation showing how conical nodes arise from crossing between nodes in the two separable electronic projections[26] applies at sufficiently short-range. These observations for the lowest eigenstates suggest that, relative to the vibronic energy, the conical intersection energy is crucial for limiting nonadiabatic eigenfunction amplitude there (at least from a diabatic perspective). An understanding of the submerged conical intersection limit with lower symmetry may be useful for investigating questions about adiabatic eigenfunction behavior when there is nonadiabatic amplitude at a conical intersection[23] and examining the transition from adiabatic to nonadiabatic tunneling.[35]

The above observations about the signs of nonadiabatic nodes deserve some comment. Examples above show a closed path that encircles two conical nodes can give an electronic index of −2, 0, or 2. The sum rule suggests that two overlapping conical nodes of the same sign might merge into a second order node, that second order nodes might split into two conical nodes of the same sign, and that oppositely signed

DOI: 10.1021/acs.jpca.7b07140
J. Phys. Chem. A 2017, 121, 7401−7413

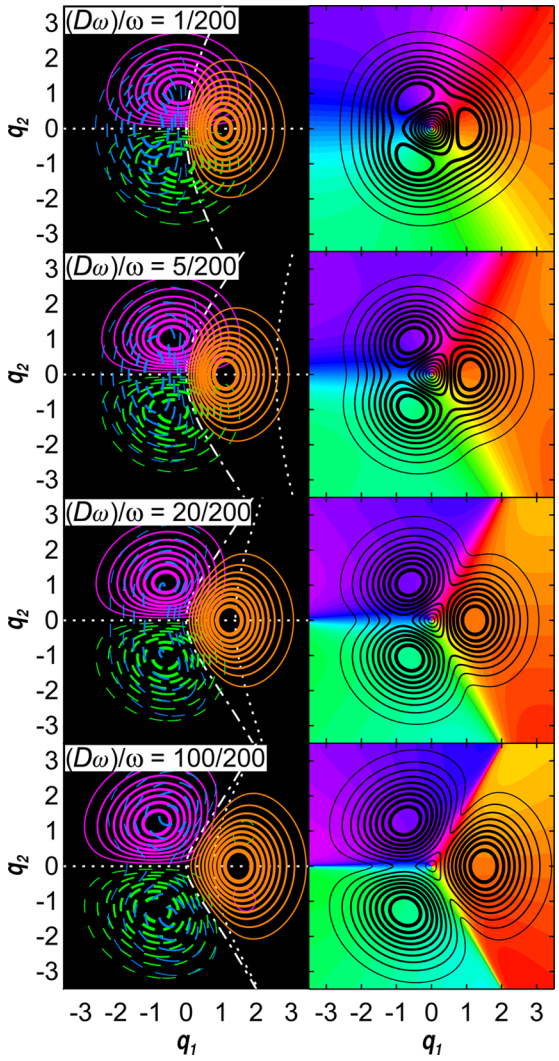

Figure 7. Coordinate dependent electronic projections (left column) and exact factorization (right column) for the (v = 1, $|j|$ = 3/2) eigenstate with $\sigma_v = -1$ as a function of the Jahn−Teller stabilization energy ($D\omega$) at a constant vibrational frequency of ω = 200 cm^{-1}. The contour interval is 10% of P_{max} for all panels and larger magnitude contours are thicker. Positive x-projection contours are solid magenta, negative x-projections are dashed green, x-projection nodes are dotted white, positive y-projections are solid orange, negative y-projections are dashed blue, and y-projection nodes are dot-dashed white. For exact factorization, colors indicate the electronic character according to the wheel in Figure 1. Rows from top to bottom show ($D\omega$) = 1 cm^{-1} (E_{zp} = 198 cm^{-1}, $E_{v=1,j=3/2}$ = 396 cm^{-1}); ($D\omega$) = 5 cm^{-1} (E_{zp} = 190 cm^{-1}, $E_{v=1,j=3/2}$ = 381 cm^{-1}); ($D\omega$) = 20 cm^{-1} (E_{zp} = 163 cm^{-1}, $E_{v=1,j=3/2}$ = 335 cm^{-1}); and ($D\omega$) = 100 cm^{-1} (E_{zp} = 47 cm^{-1}, $E_{v=1,j=3/2}$ = 169 cm^{-1}). The conical intersection is at E = 0 in all cases.

conical nodes can be created or annihilated as model parameters are varied. Zwanziger and Grant showed that a path enclosing 4 conical intersections with a net sign of 2 gives rise to a Renner-Teller effect.[17] This suggests that, just as conical nodes are in many ways analogous to conical intersections,[26] second order nonadiabatic nodes may be analogous to Renner−Teller intersections between electronic states.

Analogies between the dimensionality dependence of conical intersections and the dimensionality dependence of conical nodes[26] both suggest the above results may depend on the dimensionality of the Jahn−Teller conical intersection. Since electronic dimensionality determines whether the geometric phase around a finite loop is exactly equal to the Longuet-Higgins phase,[59−61] such an investigation may be delicate. We have not yet investigated the vibrational and electronic dimensionality dependence of nonadiabatic nodes at conical intersections.

CONCLUSIONS

The conical intersection with circular symmetry investigated here is submerged below the zero point level so that eigenfunctions are not confined to a single surface. The nonadiabatic eigenfunctions can have nonzero amplitude at a conical intersection. The zero point levels have their maximum amplitude near the Jahn−Teller displacement, approaching it more accurately as the Jahn−Teller displacement goes to zero. Around the conical intersection, the lowest order essential node in the nonadiabatic eigenfunctions has the form of a right circular cone, and its vertex is a node at the conical intersection. For nonadiabatic eigenfunctions, electronic indices have been defined through line integrals around simple closed counterclockwise paths and proven to be integers. Circular conical nodes and higher order nodes at the conical intersection occur with a lowest radial power law exponent equal to the absolute value of the electronic index for a sufficiently small path around the conical intersection. The total number of additional nodes surrounding the conical intersection is found to be $2|j|(v - |j| + 1/2)$ so long as the 2D harmonic oscillator vibrational quantum number v is good. Nonadiabatic nodes have a sign manifested in their electronic index, and the sign of the nonadiabatic nodes at the conical intersection is always opposite the sign of the conical intersection. The electronic index is equal to the sum of the electronic indices for all nodes inside the simple closed path. So long as the 2D harmonic oscillator vibrational angular momentum quantum number l remains good, the electronic index at a radius sufficient to enclose all of the nodes enumerated above is $\eta(C) = -\lambda l \, \mathrm{sgn}(\gamma)$, where λl governs the perturbative energy from vibrational−electronic interaction and $\mathrm{sgn}(\gamma)$ is the sign of the conical intersection. The results about nonzero amplitude at a conical intersection, the signs and electronic indices of nonadiabatic nodes, and the sum rule for the electronic indices are independent of the circular symmetry and submerged nature of the conical intersection studied here.

ASSOCIATED CONTENT

Supporting Information

The Supporting Information is available free of charge on the ACS Publications website at DOI: 10.1021/acs.jpca.7b07140.

Table of eigenstates energies and quantum numbers for several Jahn−Teller stabilization energies, figure showing the nonadiabatic eigenstates for v = 3 and v = 4, and figure showing both reflection operator eigenstates for the reversed conical intersection (PDF)

AUTHOR INFORMATION

Corresponding Author

*E-mail: david.jonas@colorado.edu. Phone: (303)492-3818. Fax (303)492-5894.

ORCID

David M. Jonas: 0000-0002-1085-8161

DOI: 10.1021/acs.jpca.7b07140
J. Phys. Chem. A 2017, 121, 7401−7413

Notes

The authors declare no competing financial interest.

■ ACKNOWLEDGMENTS

We thank Markus Pflaum (University of Colorado Department of Mathematics) for a helpful discussion of vector bundles. We thank Artur Izmaylov (Toronto) and Ben Levine (Michigan State) for helpful comments on a draft manuscript. This material is based upon work supported by the National Science Foundation under Grant No. CHE-1405050 and by the Air Force Office of Scientific Research under AFOSR Award No. FA9550-14-1-0258. Any opinions, findings, and conclusions or recommendations expressed in this material are those of the authors and do not necessarily reflect the views of the National Science Foundation.

■ REFERENCES

(1) Born, M.; Oppenheimer, R. Zur Quantentheorie Der Molekeln. *Ann. Phys. (Berlin, Ger.)* **1927**, *389*, 457−484.
(2) von Neumann, J.; Wigner, E. Uber Das Verhalten Von Eigenwerten Bei Adiabatischen Prozessen. *Phys. Z.* **1929**, *30*, 467−470.
(3) Jahn, H. A.; Teller, E. Stability of Polyatomic Molecules in Degenerate Electronic States. I. Orbital Degeneracy. *Proc. R. Soc. London, Ser. A* **1937**, *161*, 220.
(4) Moffitt, W.; Liehr, A. D. Configurational Instability of Degenerate Electronic States. *Phys. Rev.* **1957**, *106*, 1195−1200.
(5) Longuet-Higgins, H. C.; Öpik, U.; Pryce, M. H. L.; Sack, R. A. Studies of the Jahn-Teller Effect II. The Dynamical Problem. *Proc. R. Soc. London, Ser. A* **1958**, *244*, 1−16.
(6) Berry, M. V. Quantal Phase Factors Accompanying Adiabatic Changes. *Proc. R. Soc. London, Ser. A* **1984**, *392*, 45−57.
(7) Simon, B. Holonomy, the Quantum Adiabatic Theorem, and Berry's Phase. *Phys. Rev. Lett.* **1983**, *51*, 2167−2170.
(8) Longuet-Higgins, H. C., Some Recent Developments in the Theory of Molecular Energy Levels. In *Advances in Spectroscopy*, Thompson, H., Ed. Interscience Publishers Inc: New York, 1961; Vol. *2*, pp 429−472.
(9) Hagelberg, F. *Electron Dynamics in Molecular Interactions*; Imperial College Press: London, 2014.
(10) Atchity, G. J.; Xantheas, S. S.; Ruedenberg, K. Potential Energy Surfaces near Intersections. *J. Chem. Phys.* **1991**, *95*, 1862−1876.
(11) Bernardi, F.; Olivucci, M.; Robb, M. A. Potential Energy Surface Crossings in Organic Photochemistry. *Chem. Soc. Rev.* **1996**, *25*, 321−328.
(12) Levine, B. G.; Martinez, T. J. Isomerization through Conical Intersections. *Annu. Rev. Phys. Chem.* **2007**, *58*, 613−634.
(13) Matsika, S.; Krause, P. Nonadiabatic Events and Conical Intersections. *Annu. Rev. Phys. Chem.* **2011**, *62*, 621−643.
(14) Yarkony, D. R. Nonadiabatic Quantum Chemistry—Past, Present, and Future. *Chem. Rev.* **2012**, *112*, 481−498.
(15) Englman, R. *The Jahn-Teller Effect in Molecules and Crystals*; Wiley-Interscience: London, 1972.
(16) Koppel, H.; Domcke, W.; Cederbaum, L. S. Multimode Molecular-Dynamics Beyond the Born-Oppenheimer Approximation. In *Advances in Chemical Physics*; Advances in Chemical Physics, Vol. *57*; John Wiley & Sons, Inc.: Hoboken, NJ, 1984; pp 59−246, DOI: 10.1002/9780470142813.ch2.
(17) Zwanziger, J. W.; Grant, E. R. Topological Phase in Molecular Bound States: Application to the $E\otimes e$ System. *J. Chem. Phys.* **1987**, *87*, 2954−2964.
(18) Applegate, B. E.; Barckholtz, T. A.; Miller, T. A. Explorations of Conical Intersections and Their Ramifications for Chemistry through the Jahn-Teller Effect. *Chem. Soc. Rev.* **2003**, *32*, 38−49.
(19) Bersuker, I. B. *The Jahn-Teller Effect*. Cambridge University Press: Cambridge, U.K., 2006.
(20) Hunter, G. Conditional Probability Amplitudes in Wave Mechanics. *Int. J. Quantum Chem.* **1975**, *9*, 237−242.
(21) Hunter, G. Nodeless Wave-Functions and Spiky Potentials. *Int. J. Quantum Chem.* **1981**, *19*, 755−761.
(22) Cederbaum, L. S. The Exact Molecular Wavefunction as a Product of an Electronic and a Nuclear Wavefunction. *J. Chem. Phys.* **2013**, *138*, 224110.
(23) Meek, G. A.; Levine, B. G. Wave Function Continuity and the Diagonal Born-Oppenheimer Correction at Conical Intersections. *J. Chem. Phys.* **2016**, *144*, 184109.
(24) Abedi, A.; Maitra, N. T.; Gross, E. K. U. Exact Factorization of the Time-Dependent Electron-Nuclear Wave Function. *Phys. Rev. Lett.* **2010**, *105*, 123002.
(25) Gidopoulos, N. I.; Gross, E. K. U. Electronic Non-Adiabatic States: Towards a Density Functional Theory Beyond the Born-Oppenheimer Approximation. *Philos. Trans. R. Soc., A* **2014**, *372*, 20130059.
(26) Foster, P. W.; Peters, W. K.; Jonas, D. M. Nonadiabatic Eigenfunctions Can Have Conical Nodes. *Chem. Phys. Lett.* **2017**, *683*, 268−275.
(27) Czub, J.; Wolniewicz, L. On the Non-Adiabatic Potentials in Diatomic-Molecules. *Mol. Phys.* **1978**, *36*, 1301−1308.
(28) Peters, W. K.; Tiwari, V.; Jonas, D. M. Nodeless Vibrational Amplitudes and Quantum Nonadiabatic Dynamics in the Nested Funnel for a Pseudo Jahn-Teller Molecule or Homodimer. *J. Chem. Phys.* **2017**, submitted.
(29) Judd, B. R. Exact Solutions to a Class of Jahn-Teller Systems. *J. Phys. C: Solid State Phys.* **1979**, *12*, 1685−1692.
(30) Farrow, D. A.; Qian, W.; Smith, E. R.; Ferro, A. A.; Jonas, D. M. Polarized Pump-Probe Measurements of Electronic Motion Via a Conical Intersection. *J. Chem. Phys.* **2008**, *128*, 144510.
(31) Farrow, D. A.; Smith, E. R.; Qian, W.; Jonas, D. M. The Polarization Anisotropy of Vibrational Quantum Beats in Resonant Pump-Probe Experiments: Diagrammatic Calculations for Square Symmetric Molecules. *J. Chem. Phys.* **2008**, *129*, 174509.
(32) Kitney-Hayes, K. A.; Albrecht-Ferro, A. W.; Tiwari, V.; Jonas, D. M. Two-Dimensional Fourier Transform Electronic Spectroscopy at a Conical Intersection. *J. Chem. Phys.* **2014**, *140*, 124312.
(33) Ryabinkin, I.; Joubert-Doriol, L.; Izmaylov, A. F. When Do We Need to Account for the Geometric Phase in Excited State Dynamics? *J. Chem. Phys.* **2014**, *140*, 214116.
(34) Ryabinkin, I.; Izmaylov, A. F. Geometric Phase Effects in Dynamics near Conical Intersections: Symmetry Breaking and Spatial Localization. *Phys. Rev. Lett.* **2013**, *111*, 220406.
(35) Xie, C.; Kendrick, B. K.; Yarkony, D. R.; Guo, H. Constructive and Destructive Interference in Nonadiabatic Tunneling Via Conical Intersections. *J. Chem. Theory Comput.* **2017**, *13*, 1902−1910.
(36) Xie, C.; Yarkony, D. R.; Guo, H. Nonadiabatic Tunneling Via Conical Intersections and the Role of the Geometric Phase. *Phys. Rev. A: At., Mol., Opt. Phys.* **2017**, *95*, 022104.
(37) Hougen, J. T. Vibronic Interactions in Molecules with a Fourfold Symmetry Axis. *J. Mol. Spectrosc.* **1964**, *13*, 149−167.
(38) Landau, L. D.; Lifschitz, E. M. *Quantum Mechanics*, 3rd ed.; Pergamon Press: New York, 1977.
(39) Child, M. S.; Longuet-Higgins, H. C. Studies of the Jahn-Teller Effect III. The Rotational and Vibrational Spectra of Symmetric Top Molecules in Electronically Degenerate States. *Philos. Trans. R. Soc., A* **1961**, *254*, 259−294.
(40) Child, M. S. Studies of the Jahn-Teller Effect IV. The Vibrational Spectra of Spin-Degenerate Molecules. *Philos. Trans. R. Soc., A* **1962**, *255*, 31−53.
(41) Child, M. S. Anomalous Spectroscopic Properties Accompanying a Weak Dynamic Jahn-Teller Effect. *J. Mol. Spectrosc.* **1963**, *10*, 357−365.
(42) Marcus, R. A. Electron Transfer Reactions in Chemistry: Theory and Experiment (Nobel Lecture). *Angew. Chem., Int. Ed. Engl.* **1993**, *32*, 1111−1121.
(43) Mead, C. A.; Truhlar, D. G. On the Determination of Born−Oppenheimer Nuclear Motion Wave Functions Including Complications Due to Conical Intersections and Identical Nuclei. *J. Chem. Phys.* **1979**, *70*, 2284−2296.

DOI: 10.1021/acs.jpca.7b07140
J. Phys. Chem. A 2017, 121, 7401−7413

(44) Oka, T. Vibration—Rotation Interaction in Symmetric-Top Molecules and the Splitting between A_1 and A_2 Levels. *J. Chem. Phys.* **1967**, *47*, 5410−5426.
(45) Papousek, D.; Aliev, M. R. *Molecular Vibrational-Rotational Spectra*; Elsevier Scientific: New York, 1982.
(46) Smith, E. R.; Farrow, D. A.; Jonas, D. M. Response Functions for Dimers and Square Symmetric Molecules in Four-Wave-Mixing Experiments with Polarized Light. *J. Chem. Phys.* **2005**, *123*, 044102.
(47) Smith, E. R.; Farrow, D. A.; Jonas, D. M. Publisher's Note: ″Response Functions for Dimers and Square Symmetric Molecules in Four-Wave-Mixing Experiments with Polarized Light″ [J. Chem. Phys. **123**, 044102 (2005)]. *J. Chem. Phys.* **2005**, *123*, 179902.
(48) Smith, E. R.; Farrow, D. A.; Jonas, D. M. Erratum: ″Response Functions for Dimers and Square Symmetric Molecules in Four-Wave-Mixing Experiments with Polarized Light″ [J. Chem. Phys. **123**, 044102 (2005)]. *J. Chem. Phys.* **2008**, *128*, 109902.
(49) Clinton, W. L.; Rice, B. Reformulation of the Jahn-Teller Theorem. *J. Chem. Phys.* **1959**, *30*, 542−546.
(50) Landau, L. D.; Lifschitz, E. M. *Mechanics*, 3rd ed.; Pergamon Press: New York, 1976.
(51) Arnold, V. I. *Mathematical Methods of Classical Mechanics*, 1st ed.; Springer: New York, 1978.
(52) DiLauro, C.; Mills, I. M. Coriolis Interactions About *X-Y* Axes in Symmetric Tops. *J. Mol. Spectrosc.* **1966**, *21*, 386−413.
(53) Hougen, J. T. *The Calculation of Rotational Energy Levels and Rotational Line Intensities in Diatomic Molecules*; National Bureau of Standards Monograph 115, U.S. Government Printing Office: Washington, DC, 1970; 52 pages.
(54) Herzberg, G. H. *Infrared and Raman Spectra of Polyatomic Molecules*; Krieger: Malabar, FL, 1991; Vol. *II*.
(55) *Visual Numerics IMSL Numerical Libraries*; Rogue Wave Software: Boulder, CO.
(56) Parlett, B. N. *The Symmetric Eigenvalue Problem*; Prentice-Hall: Englewood Cliffs, NJ, 1980.
(57) The first order perturbation theory approximation in eq 8 has a conical node that is either pushed far to positive q_1 (beyond the region of accuracy) or eliminated by more accurate calculations. In Figure 3, the behavior as the Jahn−Teller stabilization energy ($D\omega$) increases is connected to a more complicated approach to the adiabatic limit.
(58) do Carmo, M. P. *Differential Geometry of Curves and Surfaces*; Prentice-Hall: Englewood Cliffs, NJ, 1976.
(59) Baer, M. On the Longuet-Higgins Phase and Its Relation to the Electronic Adiabatic−Diabatic Transformation Angle. *J. Chem. Phys.* **1997**, *107*, 2694−2695.
(60) Mead, C. A.; Truhlar, D. G. Conditions for the Definition of a Strictly Diabatic Electronic Basis for Molecular Systems. *J. Chem. Phys.* **1982**, *77*, 6090−6096.
(61) Guo, H.; Yarkony, D. R. Accurate Nonadiabatic Dynamics. *Phys. Chem. Chem. Phys.* **2016**, *18*, 26335−26352.
(62) Mead, C. A. Electronic Hamiltonian, Wave Functions, and Energies, and Derivative Coupling between Born-Oppenheimer States in the Vicinity of a Conical Intersection. *J. Chem. Phys.* **1983**, *78*, 807−814.
(63) Yarkony, D. R. Nuclear Dynamics near Conical Intersections in the Adiabatic Representation: I. The Effects of Local Topography on Interstate Transitions. *J. Chem. Phys.* **2001**, *114*, 2601−2613.
(64) Varandas, A. J. C.; Xu, Z. R. On the Behavior of Single Surface Nuclear Wavefunctions in the Vicinity of the Conical Intersection for an X_3 System. *Chem. Phys. Lett.* **2000**, *316*, 248−256.

DOI: 10.1021/acs.jpca.7b07140
J. Phys. Chem. A 2017, 121, 7401−7413